INT. J. REMOTE SENSING, 10 JANUARY, 2004,
VOL. 25, NO. 1, 215–230

Taylor & Francis
Taylor & Francis Group

Single-channel and two-channel methods for land surface temperature retrieval from DAIS data and its application to the Barrax site

J. A. SOBRINO*, J. C. JIMÉNEZ-MUÑOZ, J. EL-KHARRAZ, M. GÓMEZ, M. ROMAGUERA and G. SÒRIA

Global Change Unit, Department of Thermodynamics, Faculty of Physics, University of Valencia, Dr. Moliner 50, 46100, Burjassot, Spain

Abstract. In this paper, a methodology using a single-channel and a two-channel method is presented to estimate the land surface temperature from the DAIS (Digital Airborne Imaging Spectrometer) thermal channels 74 (8.747 μm), 75 (9.648 μm), 76 (10.482 μm), 77 (11.266 μm), 78 (11.997 μm) and 79 (12.668 μm). The land surface temperature retrieved with both methods has been validated over the Barrax site (Albacete, Spain) in the framework of the DAISEX (Digital Airborne Imaging Spectrometer Experiment) field campaigns. Prior to the validation an analysis of the DAIS data quality has been performed in order to check the agreement between *in situ* data and the values extracted from the DAIS images supplied by the DLR (German Optoelectronic Institute). Suitable differences between *in situ* and DAIS data have been found. To solve this problem a linear re-calibration of the DAIS thermal channels has been applied using two ground calibration points (bare soil and water). For the land surface temperature retrieved, rms deviations of 0.96 K using a single-channel method and 1.46 K using a two-channel method with the DAIS thermal channels 77 and 78 have been obtained considering re-calibrated data.

1. Introduction

The extensive requirement of land surface temperature (LST) for environmental studies and management activities of the Earth's resources has made the remote sensing of LST an important academic topic during the last two decades (Qin and Karnieli 1999). LST is an indication of the equilibrium thermodynamic state resulting from the energy balance of the fluxes between the atmosphere, surface and subsurface soil (Schmugge *et al.* 2002), so knowledge of LST is of great interest in many applications such as assessing water and energy budgets at the surface/atmosphere interface (Lagouarde *et al.* 1995), evapotranspiration estimation, General Circulation Models (GCM) and the greenhouse effect. However, to replace traditional temperature measurements by the ones obtained with remote sensing techniques, is it necessary to estimate LST with an adequate precision, from 2 K to estimate energy fluxes to 0.3 K to detect climatic changes (Barton 1992). For this purpose, it is necessary to solve LST estimation problems, such as calibration for

*Corresponding author; e-mail: sobrino@uv.es

International Journal of Remote Sensing
ISSN 0143-1161 print/ISSN 1366-5901 online © 2004 Taylor & Francis Ltd
http://www.tandf.co.uk/journals
DOI: 10.1080/0143116031000115210

thermal sensors, cloud detection, effective parameter definition and, mainly, atmospheric and emissivity corrections.

2. Theoretical background

On the basis of radiative transfer equation, the radiance (L_{sensor}) measured from space or aircraft in channel i may be written with a good approximation as (Becker and Li 1990a):

$$L(\theta)_{\text{sensor,i}} = L(\theta)_{\text{surface,i}}\tau(\theta)_{\text{i}} + L(\theta)^{\uparrow}_{\text{atm,i}} \tag{1}$$

where θ is the observation angle, τ_{i} is the channel total transmission of the atmosphere in channel i, $L^{\uparrow}_{\text{atm,i}}$ is the upwelling atmospheric radiance in channel i and $L_{\text{surface,i}}$ is the channel radiance observed in channel i at ground level given by:

$$L(\theta)_{\text{surface,i}} = \varepsilon(\theta)_{\text{i}} B(\theta)_{\text{i}}(T_{\text{s}}) + \left(1-\varepsilon(\theta)_{\text{i}}\right) L(\theta)^{\downarrow}_{\text{atm,i}} \tag{2}$$

In this expression, ε_{i} is the channel emissivity, $L^{\downarrow}_{\text{atm,i}}$ is the downwelling hemispheric atmospheric radiance in channel i, and $B_{\text{i}}(T_{\text{s}})$ is the channel radiance which would be measured if the surface were a blackbody ($\varepsilon = 1$) at temperature T_{s}, defined by the Planck law as:

$$B_{\text{i}}(T_{\text{s}}) = \frac{C_1}{\lambda_{\text{i}}^5 [\exp(C_2/\lambda_{\text{i}} T_{\text{s}}) - 1]} \tag{3}$$

with $C_1 = 1.19104 \times 10^8\,\text{W}\,\mu\text{m}^4\,\text{m}^{-2}\,\text{sr}^{-1}$, $C_2 = 14387.7\,\mu\text{m K}$, and λ_{i} the effective wavelength (in μm) defined as:

$$\lambda_{\text{i}} = \frac{\int_0^{\infty} \lambda f_{\text{i}}(\lambda)\,\text{d}\lambda}{\int_0^{\infty} f_{\text{i}}(\lambda)\,\text{d}\lambda} \tag{4}$$

in which $f_{\text{i}}(\lambda)$ is the spectral response of the sensor in channel i.

3. Methods for LST retrieval

3.1. *Single-channel methods*

The main goal of the single-channel method is to obtain an algorithm to retrieve LST from one thermal band of the sensor. Based on the radiative transfer equation (equations (1) and (2)) and on the linear approximation for Planck's law, it is possible to estimate LST from the DAIS thermal channel (i) using the following single-channel algorithm (Qin *et al.* 2001):

$$T_{\text{s}} = \{a_{\text{i}}(1 - C_{\text{i}} - D_{\text{i}}) + [b_{\text{i}}(1 - C_{\text{i}} - D_{\text{i}}) + C_{\text{i}} + D_{\text{i}}]T_{\text{i}} - D_{\text{i}} T_{\text{a}}\}/C_{\text{i}} \tag{5}$$

in which T_{a} is the effective mean atmospheric temperature (in K), T_{i} is the at-sensor brightness temperature (in K), $C_{\text{i}} = \varepsilon_{\text{i}}\tau_{\text{i}}$ and $D_{\text{i}} = (1-\tau_{\text{i}})[1 + (1-\varepsilon_{\text{i}})\tau_{\text{i}}]$. The coefficients a_{i} and b_{i} have been obtained from the linear approximation of the following parameter:

$$\frac{B_i(T)}{(\partial B_i(T)/\partial T)} = a_i + b_i T \tag{6}$$

This algorithm, originally developed for Landsat TM-6, has been applied to DAIS thermal channel 77 ($\lambda \approx 11.27\,\mu$m), which is similar to TM-6 (see figure 1). For this channel, the following values have been found: $a_{77} = -67.8699$ K and $b_{77} = 0.45854$, with a correlation of $r = 0.9997$ for the temperature range 273–343 K. The effective mean atmospheric temperature (T_{a}) and the atmospheric transmissivity (τ_{i}) can be

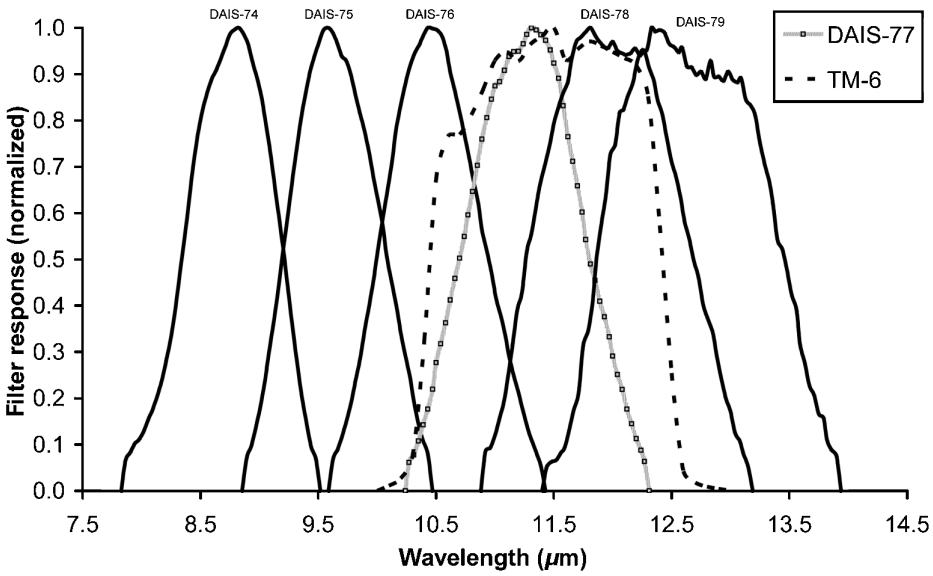

Figure 1. Thermal channels for the DAIS sensor (from 74 to 79). Landsat TM-6 channel is also represented.

obtained using the following equations:

$$T_a = 37.8807 + 0.85128\,T_o \quad (r = 0.97 \text{ and } T_o = [244.5 - 309.6\,\text{K}]) \tag{7}$$

$$\tau_{77} = 1.0449 - 0.18738\,W \quad \left(r = 0.998 \text{ and } w = \left[0.1 - 3.9\,\text{g cm}^{-2}\right]\right) \tag{8}$$

where T_o is the near-surface air temperature (in K) and W is the water vapour content (in g cm^{-2}). A detailed development and sensitivity analysis for the mono-window algorithm can be found in the reference mentioned.

3.2. *Two-channel methods*

The basis of the two-channel technique (or split-window when it is applied in the region 10–12.5 μm) is that the atmospheric attenuation suffered by the surface emitted radiance is proportional to the difference between the at-sensor radiances measured simultaneously in two different thermal channels (McMillin 1975). Many papers have used this technique to extract sea surface temperature (Deschamps and Phulpin 1980, McClain *et al.* 1985, Sobrino *et al.* 1993, etc) and land surface temperature (Price 1984, Becker and Li 1990b, Sobrino *et al.* 1991, Prata 1993, Sobrino *et al.* 1994, etc). In this paper the following two-channel algorithm is proposed, which takes into account the emissivity and water vapour effects:

$$T_s = T_i + a_0\left(T_i - T_j\right) + a_2\left(T_i - T_j\right)^2 + (a_3 + a_4 W)(1 - \varepsilon) + (a_5 + a_6 W)\Delta\varepsilon + a_1 \tag{9}$$

where T_s is the surface temperature (in K), T_i and T_j are the at-sensor brightness temperatures of the different thermal DAIS channels (in K), $\varepsilon = (\varepsilon_i + \varepsilon_j)/2$ and $\Delta\varepsilon = (\varepsilon_i - \varepsilon_j)$ are the mean effective emissivity and the emissivity difference, W is the total atmospheric water vapour (in g cm^{-2}) and finally, a_i are the numerical coefficients of the two-channel algorithm.

3.2.1. *Simulation*

To obtain the numerical coefficients given in equation (9), a simulation of the at-sensor radiometric temperatures is required. For this purpose, the MODTRAN 3.5 radiative transfer code (Abreu and Anderson 1996) has been used to predict the radiances for DAIS thermal channels (from 74 to 79) with the appropriate channel filter functions and considering the atmospheric region between the surface and the sensor altitude (from 0.7 km to 4 km). To analyse atmospheric effects a set of 60 radiosoundings data were carefully extracted from the TOVS Initial Guess Retrieval (TIGR) data base (Scott and Chedin 1981). These radiosoundings cover the variability of surface temperature (from 250 K to 320 K) and water vapour concentration (from $0.15\,g\,cm^{-2}$ to $6.71\,g\,cm^{-2}$) on a world-wide scale. The attenuation of the surface radiance has been considered by adding the uniformly mixed gases (CO_2, N_2O, CO and CH_4) and ozone, included in the standard atmospheres of the MODTRAN 3.5 code, to the water vapour taken from profiles in the TIGR radiosoundings. To accomplish this, a previous classification of the radiosoundings in terms of the total water vapour content, W ($g\,cm^{-2}$), was made according to the following groups: $0 \leqslant W \leqslant 1$, $1 \leqslant W \leqslant 2$, $2 \leqslant W \leqslant 3$, $W \geqslant 3\,g\,cm^{-2}$. Then the profiles of mixed gases from MODTRAN 3.5 for the arctic summer, US 1976, the mid-latitude summer and tropical atmospheres, were added to each group. Furthermore, three observation angles covering the swath angle of the DAIS sensor (0°, 13° and 26°), and eight different emissivities obtained from the Salisbury emissivity spectral database (basalt, sea, schiss, grass, dry grass, conifers, sand and slime) were considered (Salisbury and D'Aria, 1992). Once the simulations were made, the numerical coefficients for equation (9) were obtained using the Levenberg-Marquardt method, which is a modification of the Gauss-Newton algorithm. Table 1 shows the standard deviations associated to the statistical fit carried out to obtain the split-window coefficients ($\sigma_{simulation}$), and figure 2 illustrates the atmospheric transmissivity values obtained for the different DAIS thermal channels (from 74 to 79). This figure shows that channel 79 presents the lowest values for transmissivity, while for small values of water vapour content channels 75, 76 and 77 present the higher values for atmospheric transmissivity.

3.2.2. *Sensitivity analysis*

Taking into account error theory, it is possible to calculate the theoretical error due to the radiometric temperatures (noise), emissivity and water vapour

Table 1. Standard deviation values obtained in the two–channel algorithm simulation ($\sigma_{simulation}$).

Channel	74	75	76	77	78	79
74	–	0.56	1.03	1.02	0.80	0.42
75	0.56	–	0.67	0.60	0.47	0.29
76	1.03	0.67	–	1.38	0.99	0.81
77	1.02	0.60	1.38	–	0.47	0.59
78	0.80	0.47	0.99	0.47	–	0.87
79	0.42	0.29	0.81	0.59	0.87	–

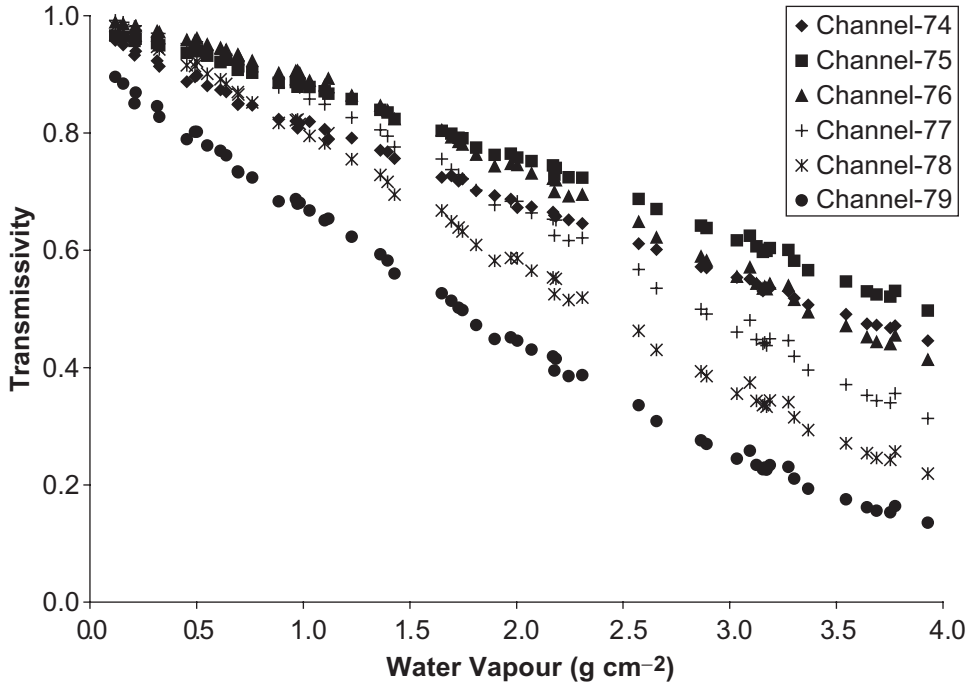

Figure 2. Simulated atmospheric transmissivity values obtained for the different DAIS thermal channels.

indeterminations using the following equation:

$$\sigma_{\text{theory}} = \sqrt{\delta^2_{\text{noise}} + \delta^2_{\text{emissivity}} + \delta^2_W} \tag{10}$$

with

$$\delta_{\text{noise}} = \sqrt{\left(\frac{\partial T_s}{\partial T_i}\right)^2 e^2(T_i) + \left(\frac{\partial T_s}{\partial T_j}\right)^2 e^2(T_j)} \tag{11}$$

$$\delta_{\text{emissivity}} = \sqrt{\left(\frac{\partial T_s}{\partial \varepsilon}\right)^2 e^2(\varepsilon) + \left(\frac{\partial T_s}{\partial \Delta\varepsilon}\right)^2 e^2(\Delta\varepsilon)} \tag{12}$$

$$\delta_W = \left(\frac{\partial T_s}{\partial W}\right) e(W) \tag{13}$$

Therefore, the total error of the LST obtained with the two-channel algorithm can be calculated using:

$$\sigma_{\text{total}} = \sqrt{\sigma^2_{\text{simulation}} + \sigma^2_{\text{theory}}} \tag{14}$$

To apply these equations, the following indeterminations have been considered: $e(T_i) = e(T_j) = 0.1$ K for the radiometric temperatures, $e(\varepsilon) = 0.005$ for emissivity values and $e(W) = 0.5\,\text{g cm}^{-2}$ for the atmospheric water vapour content. The results obtained for the total error are shown in §7.

4. DAISEX field campaigns

The European Space Agency (ESA) carries out a number of airborne campaigns to support geophysical algorithm development, calibration/validation and the simulation of future spaceborne Earth observation missions. The Digital Airborne Imaging Spectrometer Experiment that was achieved in 1998, 1999 and 2000 (DAISEX'98, DAISEX'99 and DAISEX'00) in the Barrax site (Albacete, Spain) are samples of these campaigns. The Barrax site is situated in the west of the province of Albacete, 28 km from the capital town (39°3′ N, 2°6′ W). The dominant cultivation in the 10 000 ha area is approximately 65% dry land (of which 67% are winter cereals and 33% fallow land) and 35% irrigated land (corn 75%; barley/sunflower 15%; alfalfa 5%; onions 2.9%; vegetables 2.1%). Moreover, the University of Castilla-La Mancha, through the 'Escuela Técnica Superior de Ingenieros Agrónomos', operates three agro-meteorological stations in the study area of Barrax (Moreno *et al.* 2001).

4.1. *The DAIS sensor*

The Digital Airborne Imaging Spectrometer, DAIS 7915 (or simply DAIS), is a 79-channel high resolution optical spectrometer which collects information from the Earth's surface in the 0.4–13 μm wavelength region while scanning from an aircraft, electronically processes this data into digital format consisting of 16-bit words, and records these digital data on a cartridge recorder. The DAIS scan mechanism is a Kennedy type where a cubic polygon mirror scans the terrain below through the opened window hatch in the bottom of the aircraft. The scan mirror rotates anti-clockwise with respect to the aircraft heading to provide a ground element cross track scanning motion while the forward motion of the aircraft provides a requested line-by-line scan. The most relevant geometric parameters are the IFOV (Instantaneous Field of View), 3.3 mrad, and the swath angle, ± 26 degrees. From the 79 channels, six work in the 8–12 μm region (from 74 to 79, with the next effective wavelengths: 8.747 μm, 9.648 μm, 10.482 μm, 11.266 μm, 11.997 μm and 12.668 μm respectively) with a bandwidth of 0.9 μm, which can be used for the retrieval of temperature and emissivity of the land surface objects (Müller *et al.* 2001) (see figure 3).

4.2. *Geometric and atmospheric correction for DAIS images*

The DLR (German Aerospace Center) has provided us with DAIS images geometric and atmospherically corrected, with at-surface radiance values. These two corrections have been carried out with the ATCOR4 model, which performs the combined atmospheric and topographic correction accounting for the angular and elevation dependence of the atmospheric correction functions and calculates surface reflectance (solar spectral region) and surface temperature (thermal region) based on the geocoded and orthorectified imagery (Richter 2001).

4.3. *Surface radiometric measurements*

Surface radiometric temperature measurements were collected at the Barrax site during the days of 3 and 4 July 1999, corresponding to the days when airborne acquisitions took place. The main test surfaces used for ground measurements include the following: bare soil, alfalfa, non-irrigated barley and water (sky

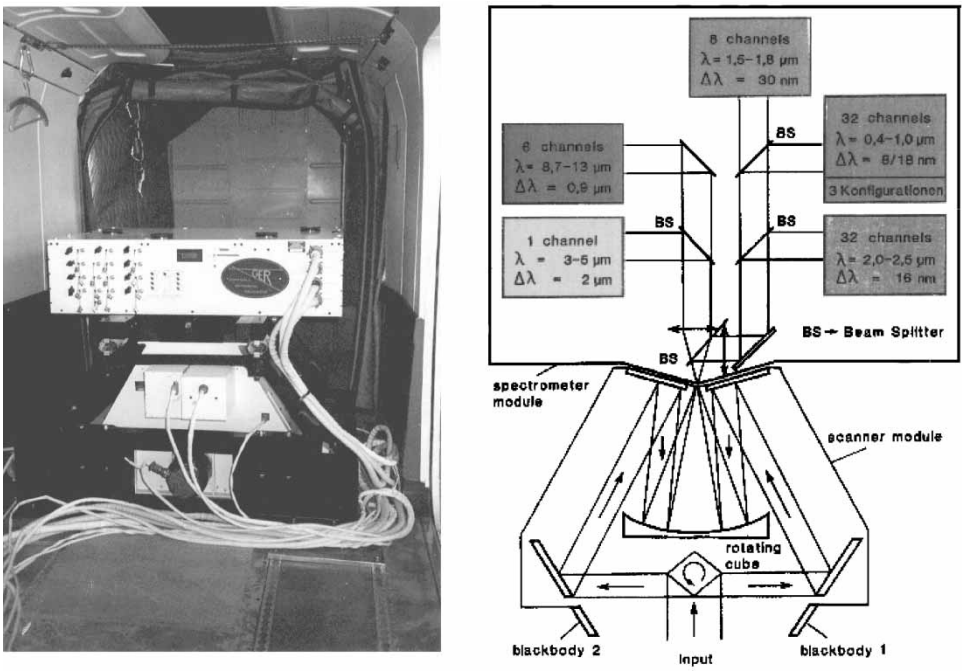

Figure 3. The DAIS sensor and its design.

temperature with the filed radiometers was also measured to estimate atmospheric radiance). In the thermal infrared domain (8–14 μm), various instruments were used that include fixed FOV—single band or multi bands radiometers. In addition, a black body was used for calibration purposes (see table 2). Emissivity values were also measured over the different test surfaces using the box method (Nerry *et al.* 1990) (see table 3), and various *in situ* radiosoundings were launched simultaneously with the over flight of the DAIS sensor (González *et al.* 2001). All these values can be used to obtain *in situ* land surface temperature (T_s) from equation (2) taking into account that $L_{\text{surface}} = B\left(T^{\text{in situ}}_{\text{radiometric}}\right)$ and $L^{\uparrow}_{\text{atm}} \cong B\left(T_{\text{sky}}\right)$.

5. On-ground re-calibration of the DAIS thermal channels

An analysis of the data quality for the DAIS sensor was carried out as a previous step of LST retrieval. For this purpose, a comparison between *in situ*

Table 2. Thermal infrared instrument characteristics.

Model	Spectral bands (μm)	Range of temperature (°C)	Accuracy (°C)	FOV (°)
Cimel CE 312	8–13 8.2–9.2 10.3–11.3 11.5–12.5	−80 to 60	0.1	10
Everest 3000.4ZLC	8–14	−30 to 100	0.2	4
Raytek	8–14	−30 to 100	0.2	8
Calibration source:				
EVEREST 1000		0 to 60	0.1	

Table 3. Emissivity values measured with the box method in the 8–13 μm region (σ: standard deviation).

Plot	Emissivity	σ
Bare soil	0.966	0.003
Alfalfa	0.996	0.005
Corn	0.974	0.016
Non-irrigated barley	0.971	0.006

at-surface radiances and the ones extracted from the DAIS images provided by the DLR has been made. The *in situ* at-surface radiances for each DAIS thermal channel have been obtained using equation (2), in which T_s is the *in situ* land surface temperature (as described in the previous section), and the spectral emissivities (see table 4) and the downwelling atmospheric radiances values have been obtained with the help of the Salisbury spectra (filtered for the DAIS thermal channels) and using the *in situ* radiosoundings as input data in the MODTRAN 3.5 code respectively. To extract the values from the DAIS images, a mean value for a 4×4 pixels box centred at the field measurements plot has been considered. The results show important differences between *in situ* and DAIS data, as is illustrated in figure 4. These differences depend on the DAIS thermal channels and on the DAIS flight, so a generalized correction cannot be applied. To solve this problem a linear re-calibration of the DAIS thermal channels is proposed using two calibration points located at the study area: bare soil (hot point) and water (cold point). With these two points, it is possible to obtain the following expression:

$$L_i^{\text{calibrated}}{}_{\text{surface}} = \text{GAIN}_i L_i^{\text{non-calibrated}}{}_{\text{surface}} + \text{OFFSET}_i \tag{15}$$

The gain and offset values obtained for each DAIS thermal channel and for each flight are given in table 5. However, when equation (15) is applied to obtain re-calibrated data over plots that have not been chosen as calibration points (for instance, non-irrigated barley and alfalfa), there is not a good agreement between *in situ* data and re-calibrated data extracted from DAIS images (see table 6). For this reason, to validate the LST retrieved with the different methods proposed in the paper, only the calibration plots will be considered (bare soil and water).

6. Results, validation and discussion

A comparison between *in situ* and retrieved LST over re-calibrated points (water and bare soil) using a single-channel and a two-channel method has been carried out in order to validate the algorithms proposed. To obtain LST with a

Table 4. Spectral emissivity values obtained from the Salisbury spectra.

Channel	Bare soil	Water
74	0.955	0.984
75	0.961	0.988
76	0.970	0.991
77	0.967	0.990
78	0.968	0.986
79	0.972	0.983

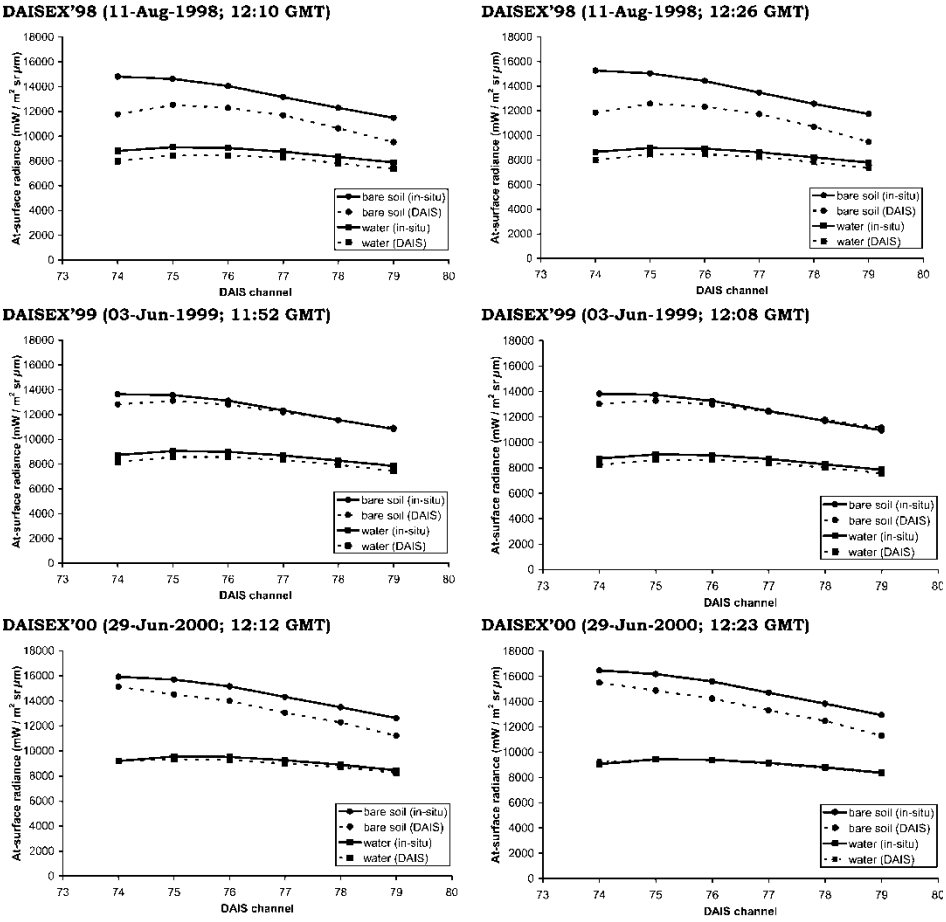

Figure 4. Comparison between *in situ* and DAIS at-surface radiances.

single-channel method, equation (5) and DAIS thermal channel 77 ($\lambda_{\text{eff}} \cong 11.3\ \mu$m) have been used. The following data are required to apply this method:

(i) *at-sensor brightness temperature* ($T_i = T_{77}$), which can be easily obtained transforming the at-sensor radiances measured by the DAIS sensor using Planck's law;
(ii) *water vapour content* (W), which can be estimated from the *in situ* radiosoundings (González *et al*. 2001) (if *in situ* radiosoundings are not available, a typical value for a mid-latitude summer atmosphere can be chosen);
(iii) *near-surface air temperature* (T_o), measured in the meteorological stations; and
(iv) *emissivity* ($\varepsilon_i = \varepsilon_{77}$), given in table 4.

In Table 7 results for validation using the single-channel method are shown, with a rms deviation (rmsd) of 0.96 K. As commented before, the mono-window algorithm proposed in this paper was developed for Landsat TM-6. It should be noted that there are two main differences between Landsat TM-6 and DAIS channel 77: (i) the filter responses are not exactly the same and (ii) the Landsat

Table 5. Gain and offset (in $mW\,m^{-2}\,sr^{-1}\,\mu m^{-1}$) for the DAIS flights carried out during the DAISEX field campaigns.

(a) 11 August 1998

	12:10 GMT		12:26 GMT	
Channel	Gain	Offset	Gain	Offset
74	1.5797	−3796	1.7124	−5028
75	1.3538	−2329	1.4747	−3504
76	1.3037	−1961	1.4204	−3095
77	1.2927	−1951	1.3882	−2811
78	1.4008	−2617	1.5168	−3653
79	1.6596	−4310	1.8445	−5728

(b) 3 June 1999

	11:52 GMT		12:08 GMT	
Channel	Gain	Offset	Gain	Offset
74	1.0541	117	1.0600	9
75	0.9957	520	1.0034	417
76	0.9757	629	0.9850	483
77	0.9447	823	0.9432	785
78	0.9110	1047	0.9045	1037
79	0.8601	1452	0.8617	1326

(c) 4 June 1999

	08:01 GMT		08:16 GMT	
Channel	Gain	Offset	Gain	Offset
74	1.0842	−217	1.2103	−1244
75	1.1975	−1413	1.2153	−1539
76	0.9889	378	1.0887	−456
77	1.0079	101	1.1023	−674
78	0.8991	1033	0.9615	554
79	0.8394	1462	0.9464	671

(d) 4 June 1999

	14:58 GMT		15:11 GMT	
Channel	Gain	Offset	Gain	Offset
74	1.0646	−216	1.0952	−668
75	1.0103	129	1.0432	−314
76	0.9693	478	1.0176	−91
77	0.9588	475	0.9841	171
78	0.9118	835	0.9302	649
79	0.8644	1253	0.8870	920

(e) 29 June 2000

	12:12 GMT		12:23 GMT	
Channel	Gain	Offset	Gain	Offset
74	1.1405	−1326	1.1895	−1979
75	1.1857	−1514	1.2322	−2152
76	1.2020	−1653	1.2699	−2492
77	1.2454	−1937	1.3017	−2626
78	1.2853	−2294	1.3441	−2916
79	1.4145	−3235	1.5233	−4285

Table 6. Comparison between *in situ* radiometric temperature obtained in the region 8–13 μm and at-surface radiometric temperature extracted from DAIS re-calibrated images using channel 76 ($\lambda_{eff} = 10.482\,\mu$m) and channel 77 ($\lambda_{eff} = 11.266\,\mu$m).

Date (GMT)	Plot	$T_{rad}^{in\ situ}$ (K)	σ (K)	$T_{76} - T_{rad}^{situ}$ (K)	$T_{77} - T_{rad}^{situ}$ (K)
3 June 1999, 11:52	alfalfa	295.80	0.30	1.89	2.48
3 June 1999, 11:52	non-irr barley	312.49	4.47	−1.60	−2.34
3 June 1999, 12:08	non-irr barley	311.88	6.14	3.80	3.20
4 June 1999, 08:01	non-irr barley 1	296.99	0.56	−1.07	−2.60
4 June 1999, 08:01	non-irr barley 2	296.98	1.25	−1.32	−2.64
4 June 1999, 08:16	non-irr barley1	296.99	0.93	1.88	0.50
4 June 1999, 08:16	non-irr barley2	297.11	0.72	0.26	−1.23
4 June 1999, 14:58	non-irr barley	311.54	1.58	−1.83	−2.47
4 June 1999, 15:11	non-irr barley	311.14	2.96	−0.76	−1.32
bias				0.14	−0.71
σ				1.96	2.25
rmsd				1.97	2.36

TM-6 is on board a satellite (altitude $\sim$705 km) while the DAIS-77 is on board a plane (altitude $\sim$4 km). In spite of these differences, the algorithm provides good results for DAIS thermal channel 77. This is due to the similarity of the effective wavelength and bandwith for both sensors and the little effect of the atmospheric water vapour for altitudes higher than 4 km.

LST has also been obtained and validated using a two-channel method through

Table 7. Results obtained for the validation of the single-channel method (σ: standard deviation, rmsd: rms deviation).

Date	GMT	Plot	$T_s^{in\ situ}$ (K)	$T_s^{mono\text{-}window} - T_s^{situ}$ (K)
11 September 1998	12:10	bare soil	327.51	−0.20
11 September 1998	12:10	water	295.45	−0.50
11 September 1998	12:26	bare soil	329.55	−0.17
11 September 1998	12:26	water	294.60	−0.50
3 June 1999	11:52	bare soil	322.21	−0.88
3 June 1999	11:52	water	295.02	−1.24
3 June 1999	12:08	bare soil	323.07	−0.86
3 June 1999	12:08	water	295.02	−1.26
4 June 1999	08:01	bare soil	303.35	−0.05
4 June 1999	08:01	water	291.88	−0.20
4 June 1999	08:16	bare soil	307.28	−0.02
4 June 1999	08:16	water	291.81	−0.20
4 June 1999	14:58	bare soil	320.08	0.24
4 June 1999	14:58	water	293.65	−0.37
4 June 1999	15:11	bare soil	320.36	0.24
4 June 1999	15:11	water	293.23	−0.37
29 June 2000	12:12	bare soil	332.18	−0.33
29 June 2000	12:12	water	298.22	−2.42
29 June 2000	12:23	bare soil	334.41	−0.17
29 June 2000	12:23	water	297.45	−2.47
bias				−0.59
σ				0.76
rmsd				0.96 (0.61*)

*rmsd value if DAISEX-2000 data are not considered.

equation (9). This equation requires similar data to those required for the single-channel method, but in this case a combination of two at-sensor brightness temperatures (T_i, T_j) is used. So equation (9) has been applied to all the different combinations between each DAIS thermal channel (from 74 to 79). In table 8 the values for bias, standard deviation and rmsd for all the DAIS thermal channel combinations and for the same plots considered in table 7 are given. The results show that the best combination is (77–78), with a rmsd value of 1.46 K. For this combination, LST values can be obtained with the following equation, in which the simulated coefficients are given:

$$T_s = T_{77} + 2.937(T_{77} - T_{78}) + 0.8193(T_{77} - T_{78})^2 - 0.3284 + (72.094 - 13.864W)(1-\varepsilon) + (-119.592 + 25.136W)\Delta\varepsilon \quad (16)$$

The combinations (75–79), (76–77), and (78–79) are also suitable for LST retrieval, with rmsd values of 2.00 K, 1.99 K, and 1.85 K respectively. As an example, in table 9 the total errors for equation (15) are shown using the equations given in §3.2.2 and considering the bare soil and water plots for the DAISEX'99 field campaign. The results show a good agreement between the 'theoretical' error ($\sim$1.3 K) and the rmsd value ($\sim$1.5 K). Analysing the different contributions to the total errors, the noise and emissivity uncertainties give the highest values, while the water vapour uncertainty gives the lowest.

7. Application to DAIS images

The methodology explained in the paper can be applied to the DAIS images to obtain maps of land surface temperature. For this purpose emissivity maps are also necessary, so the NEM (Normalized Emissivity Method) adapted to DAIS data will be used as an input image to obtain LST (the land surface emissivity retrieval from DAIS data is not within the scope of the paper; more information about this can be found in Sobrino *et al.* 2002). Figure 5 shows the Barrax test site and figure 6 illustrates temperature maps obtained from DAIS data. Figures 6(a) and 6(b) show the at-sensor and at-surface brightness temperature maps for DAIS thermal

Table 8. Results obtained for the validation of the two-channel method using different DAIS thermal channel combinations (σ: standard deviation, rmsd: rms deviation).

Channels	Bias (K)	σ (K)	rmsd (K)
74–75	0.80	5.61	5.66
74–76	−2.33	2.42	3.36
74–77	−3.70	4.25	5.64
74–78	−3.82	4.63	6.01
74–79	−3.14	4.69	5.65
75–76	−2.94	2.53	3.89
75–77	−3.23	2.70	4.21
75–78	−2.37	1.93	3.05
75–79	−1.60	1.19	2.00
76–77	−0.42	1.95	1.99
76–78	3.35	1.22	3.57
76–79	3.03	1.53	3.40
77–78	1.02	1.05	1.46
77–79	1.62	1.58	2.26
78–79	1.21	1.40	1.85

Table 9. Total errors for the two-channel algorithms that use the 77–78 combination (LT: Local Time, rmsd: rms deviation).

Date (LT)	Plot	T_s^{situ} (K)	$T_{sw\ (77–78)}$ (K)	$\lvert\delta_{noise}\rvert$ (K)	$\lvert\delta_{emi}\rvert$ (K)	$\lvert\delta_W\rvert$ (K)	σ_{total} (K)
3 June 1999, 13:52	bare soil	322.21	325.01	0.91	0.72	0.24	1.44
3 June 1999, 13:52	water	295.02	295.44	0.64	0.72	0.03	1.26
3 June 1999, 14:08	bare soil	323.07	326.02	0.92	0.72	0.24	1.44
3 June 1999, 14:08	water	295.02	295.42	0.64	0.72	0.03	1.26
4 June 1999, 10:01	water	291.88	292.02	0.60	0.66	0.03	1.21
4 June 1999, 10:01	bare soil	303.35	303.56	0.68	0.66	0.24	1.27
4 June 1999, 10:16	water	291.81	291.96	0.60	0.66	0.03	1.21
4 June 1999, 10:16	bare soil	307.28	307.87	0.73	0.66	0.24	1.30
4 June 1999, 16:58	bare soil	320.08	322.27	0.85	0.68	0.24	1.38
4 June 1999, 16:58	water	293.65	293.99	0.61	0.68	0.03	1.22
4 June 1999, 17:11	bare soil	320.36	322.58	0.85	0.68	0.24	1.38
4 June 1999, 17:11	water	293.23	293.53	0.60	0.68	0.03	1.22
rmsd							1.30

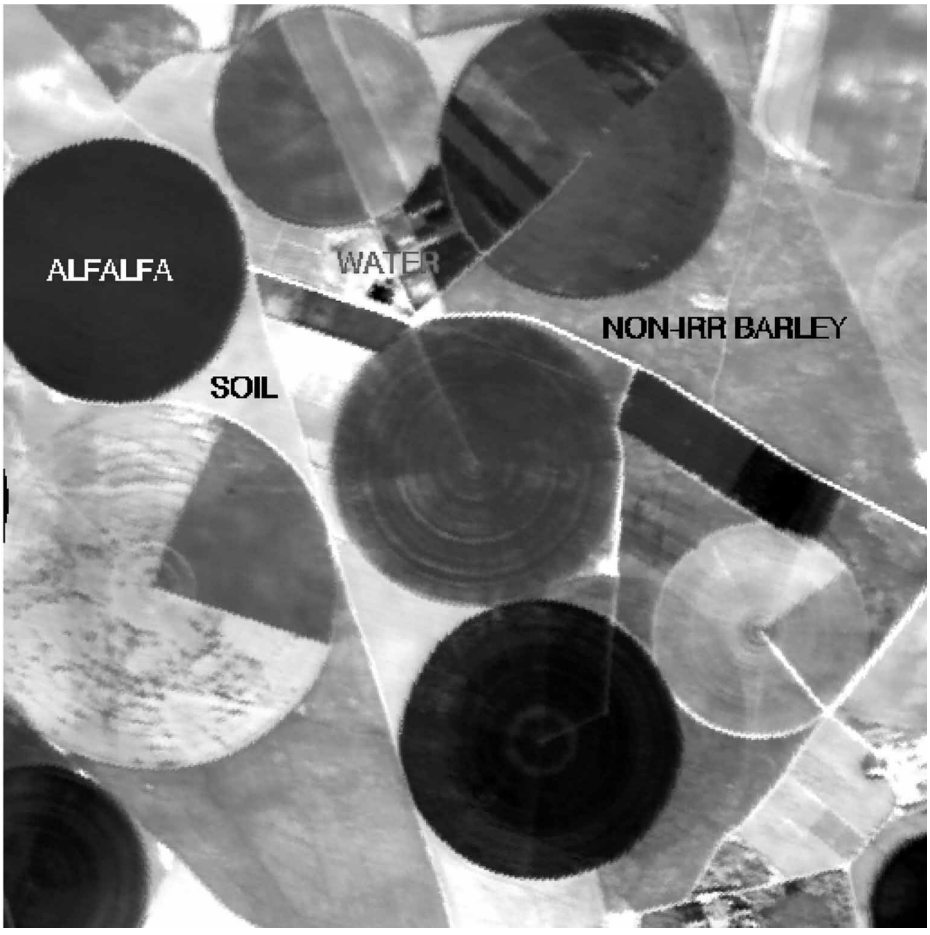

Figure 5. False colour (RGB) image using DAIS bands 10 ($\lambda = 0.659\,\mu$m), 4 ($\lambda = 0.553\,\mu$m) and 1 ($\lambda = 0.498\,\mu$m) for the Barrax test site.

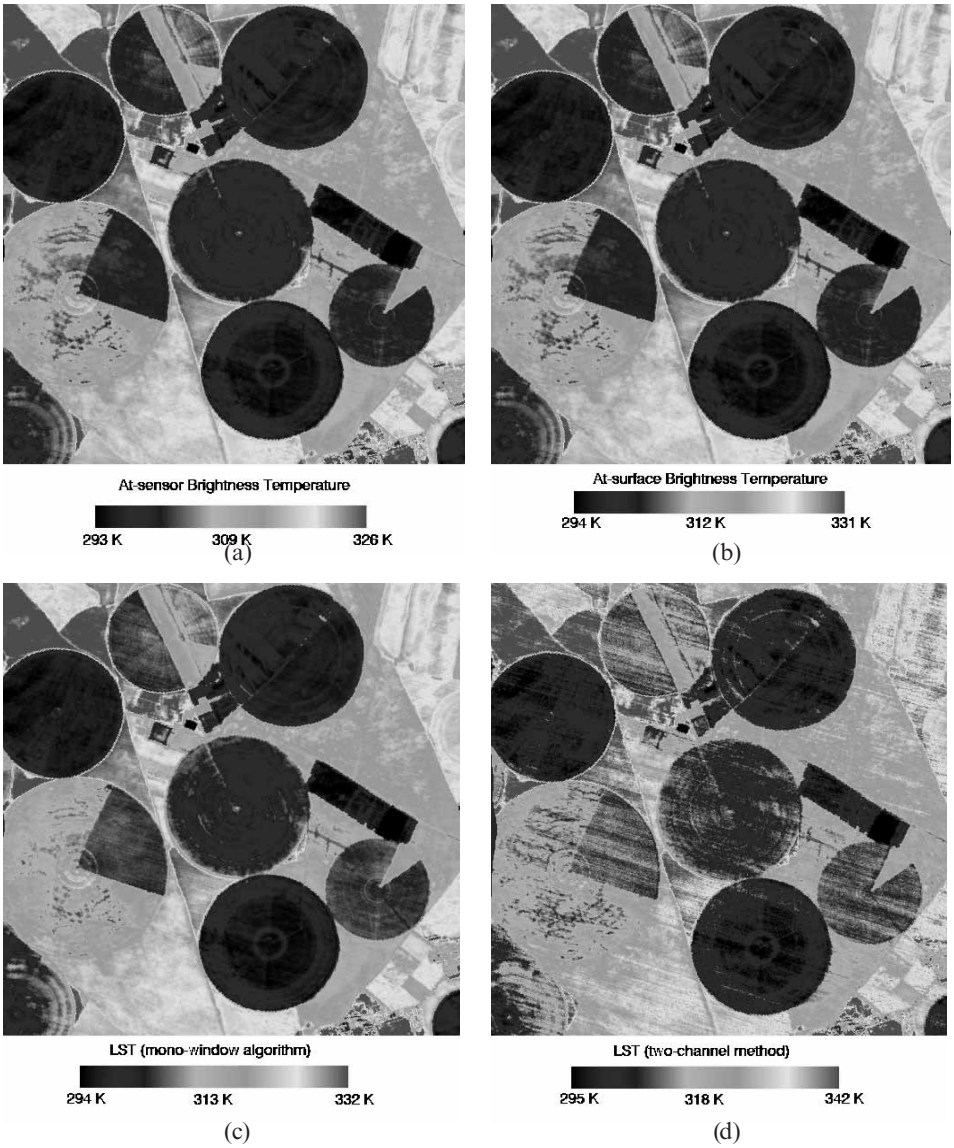

Figure 6. Temperature maps from DAIS images: (a) at-sensor brightness temperature, (b) at-surface brightness temperature, (c) LST obtained with the single-channel method (equation (5)) and (d) LST obtained with the two-channel method (equation (9)).

channel 77. The at-surface brightness temperature (called T_{ground} to avoid the confusion with the land surface temperature T_s) is obtained taking into account the expression $L_{\text{surface,i}} = B_i(T_{\text{ground}})$. Figures 6(c) and 6(d) show the land surface temperature maps with the single-channel (equation (5)) and two-channel (equation (16)) methods respectively. The differences between figures 6(a) and 6(c) (or 6(d)) are due to the atmospheric and emissivity effects. These differences are insignificant for water and vegetation plots with low temperature and high emissivity (dark colour), but not for bare soil plots with high temperature and low emissivity (red colour).

8. Conclusions

In this paper, two methodologies are proposed to estimate land surface temperature taking into account re-calibrated DAIS data: a single-channel method, in which a mono-window algorithm developed for Landsat TM-6 has been adapted to DAIS thermal channel 77, and a two-channel method, in which all the different DAIS thermal channel combinations have been considered. The validity of the models developed has been checked with the use of *in situ* data acquired over Barrax (Albacete, Spain) in the framework of the DAISEX campaigns. The results show a rmsd value of 1 K for the single-channel method. For two-channel algorithms, the channel combination (77–78) is the best, with an rmsd of 1.5 K. This result is in accordance with the channel combination used in typical split-window algorithms, as for example the channel combination AVHRR 4 and 5 on the NOAA platform.

Acknowledgments

We wish to thank the ESA (European Space Agency) for financial support (projects ESA-ESTEC 13053/NL/GD and 13390/NL/GD) and DLR for providing the DAIS images. We would also like to thank the European Union (WATERMED, Project No. ICA3-ct-1999-00015) and the Ministerio de Ciencia y Tecnología (Project REN2001-3105/CLI).

References

ABREU, L. W., and ANDERSON, G. P. (eds), 1996, The MODTRAN 2/3 Report and LOWTRAN 7 MODEL, Modtran Report, Contract F19628-91-C-0132.

BARTON, I. J., 1992, Satellite-derived sea surface temperatures – A comparison between operational, theoretical and experimental algorithms. *Journal of Applied Meteorology*, **31**, 432–442.

BECKER, F., and LI, Z.-L., 1990a, Temperature-independent spectral indices in thermal infrared bands. *Remote Sensing of Environment*, **32**, 17–33.

BECKER, F., and LI, Z.-L., 1990b, Towards a local split window method over land surfaces. *International Journal of Remote Sensing*, **11**, 36–394.

DESCHAMPS, P. Y., and PHULPIN, T., 1980, Atmospheric correction of infrared measurements of sea surface temperature using channels at 3.7, 11 and 12 μm. *Boundary Layer Meteorology*, **18**, 13–143.

GÓNZALEZ, M. C., FORTEA, J. C., MARTÍNEZ-LOZANO, J. A., UTRILLAS, M. P., PEDRÓS, R., MORENO, J., CISNEROS, J. M., and MANZANO, J. L., 2001, Measurement of Atmospheric Constituents (Ozone, Water Vapour) at Barrax. *DAISEX Final Results Workshop*, *ESTEC*, *Holland*, *15–16 March 2001*, ESA SP-499, pp. 53–61.

LAGOUARDE, J. P., KERR, Y. H., and BRUNET, Y., 1995, An experimental study of angular effects on surface temperature for various plant canopies and bare soils. *Agricultural and Forest Meteorology*, **77**, 16–190.

MCCLAIN, E. P., PICHEL, W. G., and WALTON, C. C., 1985, Comparative performance of AVHRR-based multichannel sea surface temperatures. *Journal of Geophysical Research*, **90**, 58–601.

MCMILLIN, L. M., 1975, Estimation of sea surface temperature from two infrared window measurements with different absorption. *Journal of Geophysical Research*, **80**, 511–5117.

MORENO, J., CASELLES, V., MARTÍNEZ-LOZANO, J. A., MELIÁ, J., SOBRINO, J. A., CALERA, A., MONTERO, F., and CISNEROS, J. M., 2001, The Measurments Programme at Barrax. *DAISEX Final Results Workshop*, *ESTEC*, *Holland*, *15–16 March 2001*, ESA SP-499, pp. 43–51.

MÜLLER, A., GEGE, P., and COCKS, T., 2001, The Airborne Imaging Spectrometers Used in

DAISEX. *DAISEX Final Results Workshop*, *ESTEC*, *Holland*, *15–16 March 2001*, ESA SP-499, pp. 3–6.

NERRY, F., LABED, J., and STOLL, M. P., 1990, Spectral properties of land surfaces in the thermal infrared band. Part II: Field method for spectrally averaged emissivity measurements. *Journal of Geophysical Research*, **95**, 7045–7062.

PRATA, A. J., 1993, Land surface temperatures derived from the AVHRR and ATSR, 1, Theory. *Journal of Geophysical Research*, **89**, 689–702.

PRICE, J. C., 1984, Land surface temperature measurements from the split window channels of the NOAA 7 AVHRR. *Journal of Geophysical Research*, **89**, 7231–7237.

QIN, Z., and KARNIELI, A., 1999, Progress in the remote sensing of land surface temperature and ground emissivity using NOAA-AVHRR data. *International Journal of Remote Sensing*, **20**, 2367–2393.

QIN, Z., KARNIELI, A., and BERLINER, P., 2001, A mono-window algorithm for retrieving land surface temperature from Landsat TM data and its application to the Israel-Egypt border region. *International Journal of Remote Sensing*, **22**, 3719–3746.

RICHTER, R., 2001, Atmospheric Correction Methodology for Imaging Spectrometer Data. *DAISEX Final Results Workshop*, *ESTEC*, *Holland*, *15–16 March 2001*, ESA SP-499, pp. 97–109.

SALISBURY, J. W., and D'ARIA, M., 1992, Emissivity of terrestrial materials in the 8–14 μm atmospheric window. *Remote Sensing of Environment*, **42**, 83–106.

SCHMUGGE, T., FRENCH, A., RITCHIE, J. C., RANGO, A., and PELGRUM, H., 2002, Temperature and emissivity separation from multispectral thermal infrared observations. *Remote Sensing of Environment*, **79**, 189–198.

SCOTT, N. A., and CHEDIN, A., 1981, A fast line by line method for atmospheric absorption computations: The Authomatized Atmpsheric Absorption Atlas. *Journal of Meterology*, **20**, 802–812.

SOBRINO, J. A., COLL, C., and CASELLES, V., 1991, Atmospheric correction for land surface temperature using NOAA-11 AVHRR Channels 4 and 5. *Remote Sensing of Environment*, **38**, 19–34.

SOBRINO, J. A., CASELLES, V., and COLL, C., 1993, Theoretical split window algorithms for determining the actual surface temperature. *Il Nouvo Cimento*, **16**, 219–236.

SOBRINO, J. A., LI, Z.-L., STOLL, M. P., and BECKER, F., 1994, Improvements in the split-window technique for land surface temperature determination. *IEEE Transactions on Geoscience and Remote Sensing*, **32**, 243–253.

SOBRINO, J. A., JIMÉNEZ-MUÑOZ, J. C., LABED-NACHBRAND, J., and NERRY, F., 2002, Surface emissivity retrieval from Digital Airborne Imaging Spectrometer data. *Journal of Geophysical Research*, **107**, 4729.